Ultrafast Laser-Driven Excitation Dynamics in Ne: An Ab Initio Time-Dependent R-Matrix Approach

Ultrafast Laser-Driven Excitation Dynamics in Ne: An *Ab Initio* Time-Dependent *R*-Matrix Approach

M. A. Lysaght, P. G. Burke, and H. W. van der Hart

Centre for Theoretical Atomic, Molecular and Optical Physics, Queen's University Belfast, Belfast BT7 1NN, United Kingdom

(Received 1 August 2008; published 15 December 2008)

An attosecond pump-probe scheme that combines the use of a free-electron laser pulse with an ultrashort pulse is applied in order to explore the ultrafast excitation dynamics in Ne. We describe the multielectron dynamics using a new nonperturbative time-dependent *R*-matrix theory. This theory enables the interaction of ultrashort light fields with multielectron atoms and atomic ions to be determined from first principles. By probing the emission of an inner 2*s* electron from Ne we are also able to study the bound state population dynamics during the free-electron laser pulse.

DOI: 10.1103/PhysRevLett.101.253001 PACS numbers: 31.15.A−, 32.80.Qk, 32.80.Rm

The study of atomic systems interacting with ultrashort light fields is currently attracting significant interest. Recently, the generation of extreme ultraviolet (XUV) single-cycle isolated attosecond pulses with stable and tunable carrier-envelope phases has been reported [1]. Such energetic ultrashort pulses have allowed for the real-time observation of shakeup processes in atoms [2] and have opened up the possibility of studying inner-shell dynamics on ultrafast time scales [3]. Attosecond pulses have also allowed for the profiling of the electric field of few-femtosecond laser pulses [4] and have enabled the stroboscopic study of single ionization in Ar [5].

At present, the most advanced theoretical approaches for the description of atoms irradiated by intense ultrashort light fields are approaches dedicated to two-active electron systems [6]. However, very few theoretical approaches are currently available to describe complex multielectron atoms irradiated by ultrashort light fields.

Recent experiments [2,3] have shown that the response of multielectron atoms to ultrashort pulses consists of a coherent response of many electrons, since the radiation may be sufficiently energetic to excite several electrons or cause inner-shell electrons to be emitted. Hence, to describe the response of complex atoms to ultrashort pulses, an approach needs to accurately describe both multielectron atomic structure and the multielectron response to the few-cycle light field. We thus recently introduced an *ab initio* time-dependent method that employs *R*-matrix basis functions in a box to investigate multiphoton ionization of complex atoms. The approach obtained accurate multiphoton ionization rates for Ar irradiated by a 390 nm laser pulse [7]. This approach, which consisted of an *R*-matrix inner (RMI) region only, represented the initial phase of our development of a time-dependent *R*-matrix (TDRM) theory, first proposed by Burke and Burke [8] for a 1D problem. In this Letter we describe the full 3D TDRM theory. This *ab initio* nonperturbative method can be used to accurately treat the interaction of ultrashort light fields with arbitrary multielectron atoms and atomic ions. We apply it to an ultrafast pump-probe–type experiment and use it to investigate the ultrafast ionization dynamics of Ne as a function of time delay between a few-cycle free-electron laser (FEL) "pumping" pulse and an XUV attosecond "probing" pulse. Although attosecond pulses have mainly been used as a pumping tool, an attosecond pump-probe experiment in which the attosecond pulse is used as a probe has recently been proposed [9]. However, the theoretical method employed in Ref. [9] is limited to a two-active electron problem, whereas the method applied here describes an idea for a truly multielectron attosecond pump-probe experiment.

The TDRM theory of ultrafast processes starts from the nonrelativistic time-dependent Schrödinger equation (TDSE) describing the interaction of the light field with a general $(N+1)$-electron atom or ion. Throughout our analysis we assume that the light field is linearly polarized and spatially homogeneous. Using the unitary Cayley form of the time evolution operator $\exp[-itH(t)]$ and neglecting terms of $\mathcal{O}(\Delta t^3)$, the solution of the TDSE (in atomic units) at time $t = t_{q+1}$ can then be expressed in terms of the solution at $t = t_q$ as follows:

$$[H(t_{q+1/2}) - E]\Psi(\mathbf{X}_{N+1}, t_{q+1}) = \Theta(\mathbf{X}_{N+1}, t_q), \quad (1)$$

where

$$\Theta(\mathbf{X}_{N+1}, t_q) = -[H(t_{q+(1/2)}) + E]\Psi(\mathbf{X}_{N+1}, t_q). \quad (2)$$

In Eqs. (1) and (2) $\mathbf{X}_{N+1} \equiv \mathbf{x}_1, \mathbf{x}_2, \ldots, \mathbf{x}_{N+1}$, where $\mathbf{x}_i \equiv \mathbf{r}_i\sigma_i$ are the space and spin coordinates of the ith electron, $H(t_{q+1/2})$ is the time-dependent Hamiltonian at the midpoint which is described in the length gauge throughout. In this formalism the imaginary energy defines the time step and is given by $E \equiv 2i\Delta t^{-1}$.

The solution of Eq. (1) is accomplished by partitioning configuration space into an internal and external region as in the standard *R*-matrix method [10] with the boundary at radius $r = a$. In the internal region electron exchange and electron-electron correlation effects between the ejected electron and the remaining N electrons are important, while in the external region such effects are negligible.

Hence, the ejected electron moves in the local long-range multipole potential of the residual N-electron atom or atomic ion together with the laser potential.

Since the Hamiltonian $H(t_{q+1/2})$ in Eq. (1) is not Hermitian in the internal region $r \leq a$ due to the kinetic energy term in $H(t_{q+1/2})$, we introduce the Bloch operator $\mathcal{L}$ following standard R-matrix theory [10] such that $H_{N+1} + \mathcal{L}$ is Hermitian in the internal region. We thus rewrite Eq. (1) in the internal region as

$$\Psi = (H + \mathcal{L} - E)^{-1}(\mathcal{L}\Psi + \Theta), \tag{3}$$

where for notational simplicity we have omitted the arguments in H, Ψ, and Θ. In the internal region, an R-matrix basis expansion of the wave function Ψ is adopted and we use our recently developed RMI approach [7] to set up the linear equations given by Eq. (3). Using a linear solver at each time step enables the R-matrix, $\mathbf{R}$ as defined in [8], to be calculated on the boundary $r = a$ of this region and also enables the calculation of an inhomogeneous T vector, $\mathbf{T}$ also as defined in [8].

Projecting Eq. (3) onto the channel functions $\bar{\Phi}_i^\Gamma$, which are formed by coupling the residual atom or ion states Φ_i with angular and spin functions of the ejected electron [10], and evaluating on the boundary of the internal region we obtain

$$F_p(a) = \sum_{p'=1}^{n} R_{pp'}(a)\bar{F}_{p'}(a) + T_p(a), \qquad p = 1, \ldots, n, \tag{4}$$

where the reduced radial wave functions $F_p(a)$ are defined by $F_p(a) = \langle \bar{\Phi}_i^\Gamma r_{N+1}^{-1} | \Psi \rangle'_{r_{N+1}=a}$ and the modified derivative functions $\bar{F}_p(a)$ are defined by $\bar{F}_p(a) = \frac{dF_p}{dr}|_{r=a}$. We also note that the prime on the matrix elements means that the integral is carried out over space and spin coordinates of all $N + 1$ electrons except the radial coordinate r_{N+1} of the ejected electron. Also, $\Gamma = \gamma L S M_L M_S \pi$ and the variable p in Eq. (4) represents both Γ and i.

The only unknown in Eq. (4) is $\bar{F}_p(a)$ which can be determined from the results of the external region. Hence the wave function $\Psi(\mathbf{X}_{N+1}, t_{q+1})$, which provides the starting point for the calculation in the next time step, can be determined from Eq. (4).

In the external region, we solve Eq. (1) by expanding the wave function Ψ in terms of reduced radial functions $F_p(r)$ which are analytic continuations of the functions which are defined by Eq. (4) on the boundary of the internal region. Coupled second-order differential equations satisfied by the reduced radial wave functions $F_p(r)$, which represent the motion of the electron in the pth channel, can be obtained by substituting such an expansion into Eq. (1) and projecting onto the channel functions $\bar{\Phi}_i^\Gamma$. The coupled inhomogeneous second-order differential equations can be written in matrix form as

$$(\mathbf{H} - E\mathbf{I})\mathbf{F}(r) = \boldsymbol{\theta}(r), \tag{5}$$

where the Hamiltonian matrix $\mathbf{H}$ is now defined by

$$\mathbf{H} = -\frac{1}{2}\left(\mathbf{I}\frac{d^2}{dr^2} + \mathbf{V}(r) - 2\mathbf{W}(r) + \mathbf{k}^2\right), \tag{6}$$

where $\mathbf{I}$ is the unit matrix and $\mathbf{V}(r)$ represents the combined nuclear and centrifugal potential matrix and $\mathbf{k}^2$ can be expressed in terms of the diagonal energy eigenvalue matrix $\mathbf{E_n}$ of the residual N-electron atom or ion, by the equation $\mathbf{k}^2 = -2\mathbf{E_n}$. $\mathbf{W}(r)$ is the long-range potential matrix coupling the channels as described in Ref. [11], although here we describe the laser field in the length gauge in the external region. Finally, the inhomogeneous term $\boldsymbol{\theta}(r)$ in Eq. (5) is defined for a single channel by

$$\boldsymbol{\theta}_p(r) = \langle \bar{\Phi}_i^\Gamma(\mathbf{X}_N; \hat{\mathbf{r}}_{N+1}\sigma_{N+1}) r_{N+1}^{-1} | \Theta \rangle, \tag{7}$$

where Θ has already been defined in Eq. (2) and where we have omitted the time variable in $\theta_p(r)$ and in the potential terms $\mathbf{W}(r)$ in Eq. (6) for notational convenience. The complex energy E in Eqs. (5) and (6) is measured from the lowest threshold of the residual atom or ion.

In order to solve Eq. (5), we subdivide the external region into n_s subregions and propagate the R matrix and T vector calculated at $r = a$ for a given time step across the subregions to yield the R matrix and T vector at $r = a_p$, which can then be used to propagate the wave function backwards across the n_s subregions commencing with the boundary condition $\mathbf{F}(a_p) = \mathbf{0}$.

In the sth subregion we introduce a Bloch operator $\mathcal{L}_s$ defined in Ref. [12] which is such that $\mathbf{H} + \mathcal{L}_s$ is Hermitian over the sth subregion $a_{s-1} \leq r \leq a_s$. We can then write the formal solution of Eq. (5) in the sth subregion with $a_{s-1} \leq r \leq a_s$ as

$$\mathbf{F}(r) = 2\int_{a_{s-1}}^{a_s} \mathbf{G}_s(r, r')\mathcal{L}_s\mathbf{F}(r')dr' + \mathbf{J}(r), \tag{8}$$

where

$$\mathbf{J}(r) = 2\int_{a_{s-1}}^{a_s} \mathbf{G}_s(r, r')\boldsymbol{\theta}(r')dr', \tag{9}$$

and $\mathbf{G}_s(r, r') = (\mathbf{H} + \mathcal{L}_s - E\mathbf{I})^{-1}$. We use a spectral representation of the Green function in Eqs. (8) and (9) [12], where we use a basis of B splines and solve a system of linear equations in each subregion. Evaluating Eq. (8) at $r = a_{s-1}$ and $r = a_s$ then yields the following outward propagation equations for $\mathbf{R}_s$ and $\mathbf{T}(a_s)$:

$$a_s\mathbf{R}_s = \mathbf{G}_s(a_s, a_s) - \mathbf{G}(a_s, a_{s-1})[\mathbf{G}_s(a_{s-1}, a_{s-1}) + a_{s-1}\mathbf{R}_{s-1}]^{-1}\mathbf{G}_s(a_{s-1}, a_s), \tag{10}$$

and

$$\mathbf{T}(a_s) = \mathbf{J}(a_s) + \mathbf{G}_s(a_s, a_{s-1})[\mathbf{G}_s(a_{s-1}, a_{s-1}) + a_{s-1}\mathbf{R}_{s-1}]^{-1}[\mathbf{T}(a_{s-1}) - \mathbf{J}(a_{s-1})]. \tag{11}$$

The R matrix and T vector on the boundary $r = a$ of the internal region are obtained from solving Eq. (3) in the internal region. Finally we obtain the following inward

propagation equation for the wave function:

$$\mathbf{F}(a_{s-1}) = a_{s-1}\mathbf{R}_{s-1}[\mathbf{G}_s(a_{s-1}, a_{s-1}) + a_{s-1}\mathbf{R}_{s-1}]^{-1} \times \{\mathbf{G}_s(a_{s-1}, a_s)a_s^{-1}\mathbf{R}_s^{-1}[\mathbf{F}(a_s) - \mathbf{T}(a_s)] + \mathbf{G}_s(a_{s-1}, a_{s-1})a_{s-1}^{-1}\mathbf{R}_{s-1}^{-1}\mathbf{T}(a_{s-1}) + \mathbf{J}(a_{s-1})\}. \quad (12)$$

The wave function for all values of r is then obtained from Eq. (8) and hence the inhomogeneous terms in Eqs. (2) and (11) can be calculated for the next time integration step. In this way Eq. (1) can be stepped forward in time for all positive t_q given the wave function at time $t = 0$. In order to verify the stability and accuracy of the new TDRM method we have compared wave functions irradiated by 12 eV photons obtained using the TDRM method with those obtained using the recently developed RMI method and have found excellent agreement [13].

As a means of demonstrating the capability of the TDRM method we investigate the multielectron dynamics of Ne in a proposed ultrafast pump-probe–type experiment. In this experiment we irradiate Ne with a 17 eV few-cycle FEL pulse that is resonant with the $2s^22p^53s\ ^1P^o$ excited bound state as shown in Fig. 1. During the FEL pulse, population is transferred from the $2s^22p^6\ ^1S^e$ ground state to the $2s^22p^53s\ ^1P^o$ excited state. At a given point in time during the few-cycle pulse we irradiate Ne with an XUV ultrashort pulse that has a high enough frequency to ionize the given amount of population in the $2s^22p^53s\ ^1P^o$ excited state, at that specific time, to continuum channels coupled to the $2s^12p^6\ ^2S^e$ ionic state. By varying the time delay $\Delta\tau$ between the FEL pulse and the XUV ultrashort pulse it is possible to study the time-dependent transfer of population between the ground state and resonant excited state by investigating how the population in the channels coupled to the $2s^12p^6\ ^2S^e$ ionic state varies as a function of $\Delta\tau$.

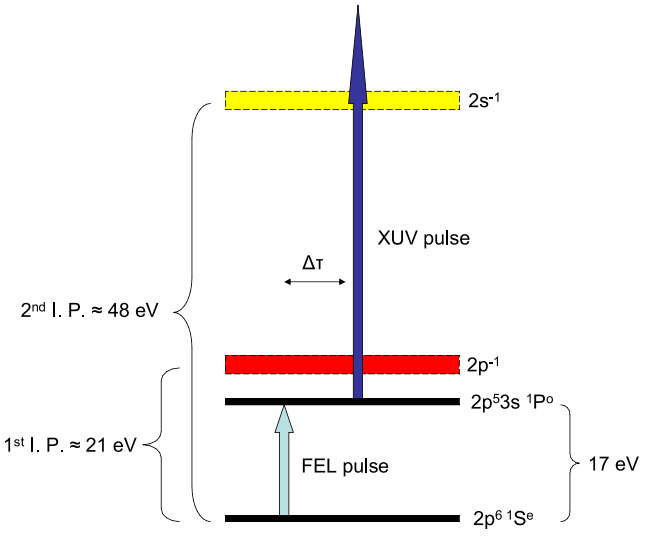

FIG. 1 (color online). Schematic of the energy level diagram for the pump-probe experiment. (I.P. denotes ionization potential.)

In the present calculations the 17 eV FEL laser pulse has a three-cycle $\sin^2$ turn-on of the electric field, 14 cycles at constant peak amplitude, followed by a three-cycle $\sin^2$ turn-off. The XUV ultrashort light pulse consists of a combination of the 15th, 17th, 19th, and 21st harmonics of 780 nm radiation and a Gaussian time envelope. The profile of the electric field can be seen in the top half of Fig. 2, where we show the position of the XUV ultrashort pulse for two different time delays. The FEL has a peak intensity of 5×10^{13} W/cm^2, and the XUV pulse has a peak intensity of 1.72×10^{12} W/cm^2.

In the internal region we use the basis developed for single-photon ionization of Ne [14], although we extend the box radius to 20 a.u., while the set of continuum orbitals contains 50–60 continuum functions for each angular momentum of the continuum electron. We include both the $1s^22s^22p^5\ ^2P^o$ ground state and the $1s^22s^12p^6\ ^2S^e$ first excited state of Ne^+ as target states. The description of Ne includes all $1s^22s^22p^5\varepsilon l$ and $1s^22s^12p^6\varepsilon l'$ channels up to $L = 9$. In the external region we propagate the R matrix and T vector outwards to a radial distance of typically 400 a.u. to prevent reflections of the wave function from the external region boundary. Each external region sector is typically 3 a.u. wide and contains 35 B splines per channel with order $k \geq 9$.

In the bottom half of Fig. 2, we show the population in the channels coupled to the $^2S^e$ ionic state as a function of time, corresponding to two different values of $\Delta\tau$ shown in the top half of Fig. 2. The population is obtained by

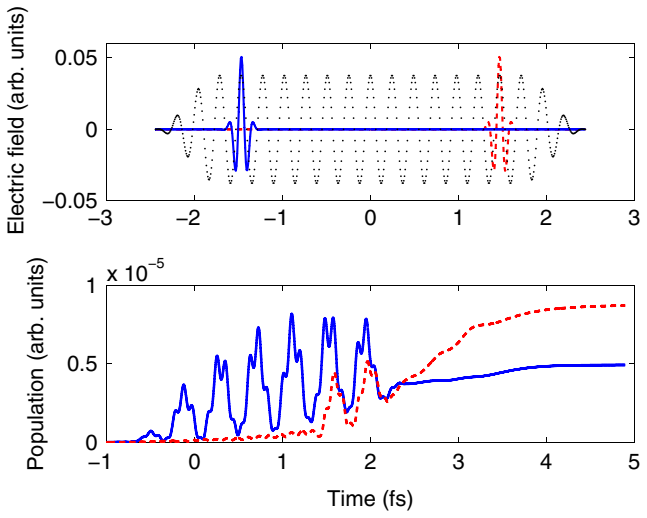

FIG. 2 (color online). Top: Schematic of the electric field. FEL field is shown as black dot. Ultrashort pulse is shown as blue solid line ($\Delta\tau = -1.5$ fs) and red dashed line ($\Delta\tau = +1.5$ fs). Bottom: Population in the channels coupled to the $^2S^e$ ionic state as a function of the time for the two different time delays between the attosecond pulse and the FEL pulse shown in the top half of the figure. The blue solid line results are for $\Delta\tau = -1.5$ fs and the red dashed line results are for $\Delta\tau = +1.5$ fs.

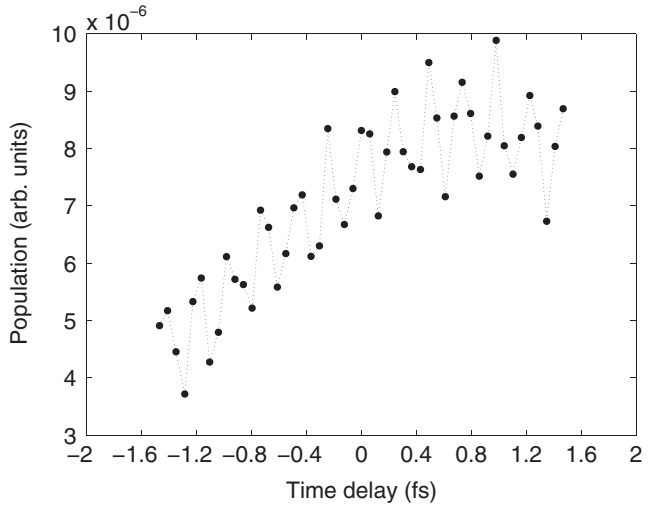

FIG. 3. Population in the channels coupled to the $2s^1 2p^6\ ^2S^e$ ionic state as a function of the time delay between the attosecond pulse and the longer 17 eV pulse. The results show the population calculated 2.5 fs after the end of the pulses.

calculating the norm of the wave function beyond $r = 50$ a.u.. As is expected, the population in channels coupled to the $^2S^e$ ionic state 2.5 fs after both pulses is greater for $\Delta\tau = +1.5$ fs than for $\Delta\tau = -1.5$ fs, as more population has been transferred from the ground state to the $2s^2 2p^5 3s\ ^1P^o$ state at this later stage in the evolution of the FEL pulse. The reason for the delayed increase in population after the end of the pulses, seen in Fig. 2, is due to the time it takes for the outgoing wave packets to reach the spatial region in which the population is calculated. The Rabi oscillation of the population for $\Delta\tau = -1.5$ fs can be explained by the fact that after ionization, due to the ultrashort pulse, most of the Ne^+ population is in the ground state. This population now interacts with the FEL pulse, leading to the observed Rabi oscillations. The large difference between the 17 eV photon energy and the core $2s^2 2p^5\ ^2P^o \rightarrow 2s^1 2p^6\ ^2S^e$ field-free transition energy $\approx$27 eV leads to rapid population and depopulation of channels coupled to the $^2S^e$ ionic state with a Rabi period $\approx$0.8 fs.

Figure 3 shows the population calculated 2.5 fs after the end of the pulses as a function of $\Delta\tau$. The population steadily increases with time, indicating a corresponding increase in the $2s^2 2p^5 3s\ ^1P^o$ population due to the ''pump'' FEL pulse. However, this increase is superimposed by a more complicated structure, with clear evidence of both oscillatory behavior and a turn-off effect at longer time delays. The oscillations have a frequency that matches the FEL photon frequency and can be explained by interference in the time domain between the electric fields associated with each pulse. When the respective fields of each pulse are out of phase with each other they interfere destructively, resulting in an effective field strength that is weaker than if the fields are in phase. This ''weaker'' pulse accounts for a reduction in the ionization from the $2s^2 2p^5 3s\ ^1P^o$ state when the fields are out of phase. As well as effectively reducing the field strength, the destructive interference of the fields results in the excited state population being driven back to the ground state. This behavior also accounts for a reduction in ionization to channels coupled to the $^2S^e$ ionic state. Conversely, constructive interference of the fields leads to an increase in population of these channels. The turn-off at large delays may be due to the pulses exciting Ne in the opposite order: the attosecond pulse excites Ne and the FEL pulse subsequently causes the emission of the $2s$ electron. This process would decrease in importance with less duration remaining for the FEL pulse.

In conclusion, we have presented a new *ab initio* time-dependent R-matrix theory for ultrafast multielectron processes. We have applied this approach to an attosecond streaking technique in order to study ultrafast excitation dynamics in Ne and have found evidence of a core excitation process occurring during the escape of the electron due to the FEL pulse. We have also studied the time-dependent transfer of population between resonantly coupled bound states of Ne during the FEL coupling field owing to the ability to include inner-shell excitations. With the current scaling of experimental techniques to higher photon energies, shorter x-ray pulse durations and increasing stability [15], along with proposals for FEL based attosecond sources [16], an accurate understanding of ultrafast inner-shell processes will increase in importance. Hence, this new method represents a timely and significant development for the accurate computation and understanding of ultrafast multielectron dynamics.

The authors thank Dr. L. A. A. Nikolopoulos for helpful discussions. M. L. was supported by Grant No. EP/E000223/1 from the U.K. EPSRC.

[1] G. Sansone *et al.*, Science **314**, 443 (2006).
[2] M. Uiberacker *et al.*, Nature (London) **446**, 627 (2007).
[3] M. Drescher *et al.*, Nature (London) **419**, 803 (2002).
[4] E. Goulielmakis *et al.*, Science **305**, 1267 (2004).
[5] J. Mauritsson *et al.*, Phys. Rev. Lett. **100**, 073003 (2008).
[6] J. S. Parker *et al.*, Phys. Rev. Lett. **96**, 133001 (2006).
[7] H. W. van der Hart, M. A. Lysaght, and P. G. Burke, Phys. Rev. A **76**, 043405 (2007).
[8] P. G. Burke and V. M. Burke, J. Phys. B **30**, L383 (1997).
[9] S. X. Hu and L. A. Collins, Phys. Rev. Lett. **96**, 073004 (2006).
[10] P. G. Burke and K. A. Berrington, *Atomic and Molecular Processes: An R-Matrix Approach* (IOP, Bristol, 1993).
[11] P. G. Burke, P. Francken, and C. J. Joachain, J. Phys. B **24**, 761 (1991).
[12] K. L. Baluja, P. G. Burke, and L. A. Morgan, Comput. Phys. Commun. **27**, 299 (1982).
[13] M. A. Lysaght *et al.* (to be published).
[14] P. G. Burke and K. T. Taylor, J. Phys. B **8**, 2620 (1975).
[15] G. D. Ninno *et al.*, Phys. Rev. Lett. **101**, 053902 (2008).
[16] A. A. Zholents and G. Penn, Phys. Rev. ST Accel. Beams **8**, 050704 (2005).